Research Article

Xinyi Gu#, Xiaoli Chen#, Xiaoxuan Tang, Zhihao Zhou, Tingting Huang, Yumin Yang*, and Jue Ling*

Pure-silk fibroin hydrogel with stable aligned micropattern toward peripheral nerve regeneration

https://doi.org/10.1515/ntrev-2021-0002
received December 22, 2020; accepted January 12, 2021

Abstract: Successful repair of long-distance peripheral nerve injuries remains a challenge in the clinic. Rapid axon growth is a key to accelerate nerve regeneration. Herein, a pure silk fibroin (SF) hydrogel with a combination of high-strength and aligned microgrooved topographic structure is reported. The hydrogels exhibit excellent mechanical properties with high strength. Good biocompatibility also allows the hydrogels to support cell survival. Significantly, the hydrogel with aligned microgrooved structures enables the aligned growth of Schwann cells. Moreover, the hydrogel holds a strong capacity for promoting axon growth and guiding neurite sprouting. Thus, this micropatterned SF hydrogel would have great potential for peripheral nerve regeneration.

Keywords: silk fibroin, hydrogel, micropattern, peripheral nerve regeneration

1 Introduction

Peripheral nerve injury is one of the most common nervous system injuries. Due to trauma, disease, or surgery, there are about 2 million new cases every year globally [1–3]. In the past decade, the use of artificial nerve grafts to repair damaged peripheral nerves has been widely studied, and significant progress has been made in the repair of short-distance nerve injury [4]. However, the successful repair of long-distance peripheral nerve injuries (>40 mm) still remains a challenge [5]. Rapid axon growth is a key to accelerate long-distance peripheral nerve regeneration [6]. The topographic structure as a key physical factor of biomedical materials can effectively regulate the microenvironment of nerve regeneration [7]. It has been reported that topographic structure can regulate the growth of nerve cells [8]. However, either the insufficient effect of topographic structures on axon growth or poor biocompatibility limits the application of these biomedical materials with topographic structures for the repair of long-distance peripheral. Moreover, one optimal dimension of aligned topographic structure on nerve repair scaffolds for promoting both rapid axon growth and Schwann cells growth has rarely been found.

Recently, micropatterned materials based on carbon nanotubes can effectively promote nerve cell culture growth [9]. Microstructures on materials created by the electrospinning technique can also potentially mimic extracellular matrix for promoting tissue regeneration [10]. Importantly, it has been found that introducing oriented microstructure into artificial nerve grafts can induce the directional migration and growth of nerve cells [11]. Oriented microstructures can also guide the rapid growth of axons crossing the damaged area, which promotes the repair and functional reconstruction of nerve [12]. Previously, it was also found that anisotropic bridge microstructure can regulate the morphology and biological function of Schwann cells [13]. The synthetic

# These authors contributed equally to this work.

*** Corresponding author: Yumin Yang,** Key Laboratory of Neuroregeneration, Neural Regeneration Co-Innovation Centre of Jiangsu Province, Jiangsu Clinical Medicine Center of Tissue Engineering and Nerve Injury Repair, Nantong University, Nantong, 226001, China, e-mail: yangym@ntu.edu.cn
*** Corresponding author: Jue Ling,** Key Laboratory of Neuroregeneration, Neural Regeneration Co-Innovation Centre of Jiangsu Province, Jiangsu Clinical Medicine Center of Tissue Engineering and Nerve Injury Repair, Nantong University, Nantong, 226001, China, e-mail: jl2016@ntu.edu.cn
Xinyi Gu, Xiaoli Chen, Xiaoxuan Tang, Zhihao Zhou, Tingting Huang: Key Laboratory of Neuroregeneration, Neural Regeneration Co-Innovation Centre of Jiangsu Province, Jiangsu Clinical Medicine Center of Tissue Engineering and Nerve Injury Repair, Nantong University, Nantong, 226001, China

matrix showed extraordinary physical properties to meet microstructural demands [14]. Synthetic hydrogel-based materials with the micro-groove structure on the surface can also effectively regulate the migration and oriented growth of Schwann cells [15]. However, poor biocompatibility usually limits the biomedical applications of these synthetic materials with a topographic structure *in vivo* [16]. Biocompatible materials, such as collagen [17], silk [18], and chitosan [19], have great potential in biomedical applications [20]. These natural biopolymers have significant advantages, such as long-term safety [21], desirable biocompatibility [22], and biodegradability [23]. However, the weak mechanical strength of most biopolymer-based scaffolds goes against the formation of artificial topographic structures [24]. Therefore, it is necessary to develop biocompatible materials with a stable topographic structure to meet current biomedical demands.

Silk fibroin (SF) has attracted considerable interest in tissue engineering [25]. SF as a natural biopolymer possesses excellent biocompatibility [26]. SF-based biomaterials hold non-immunogenic properties, which are very important for implantation [27]. Biodegradability is one of the important properties of biomaterials [28]. SF also has suitable biodegradation kinetics and solid physical strength with flexibility for biomedical applications *in vivo* [29]. For tissue repair, SF has also been shown to support cell attachment and cell survival to promote tissue regeneration [30]. For peripheral nerve regeneration, it has been reported that SF can promote the proliferation of Schwann cells [31]. Meanwhile, SF-based hydrogel can also support neuron growth for central nerve repair [32]. Previously, it was found that the direction of neuronal growth could be guided by aligned SF fibers [33]. Although SF-based hydrogel has shown lots of advantages in the field of tissue engineering, the poor mechanical properties of SF hydrogel still tolerate its practical application [34]. The addition of crosslink agents or chemical components can enhance the mechanical strength but most of these agents show potentially toxic to cells [35]. Therefore, generating SF hydrogels with the combination of high strength and desirable biocompatibility remains a challenge. In this study, we developed tough micropatterned pure-SF hydrogel with aligned microgrooved structures with three different width dimensions of 10, 30, and 50 μm, which possesses promising biocompatibility and good mechanical strength. Importantly, micropatterned pure-SF hydrogel with aligned microgrooved structures with a width of 30 μm holds strongest capacity to promote both Schwann cells growth and guide neurite sprouting for peripheral nerve regeneration (Scheme 1).

2 Materials and methods

2.1 Preparation of hydrogels

For TPSF hydrogels, 50 g of natural silk was boiled in 2 L of 0.2% w/v sodium carbonate solution for 30 min at 100°C, and then washed with ultra-pure water. The degummed

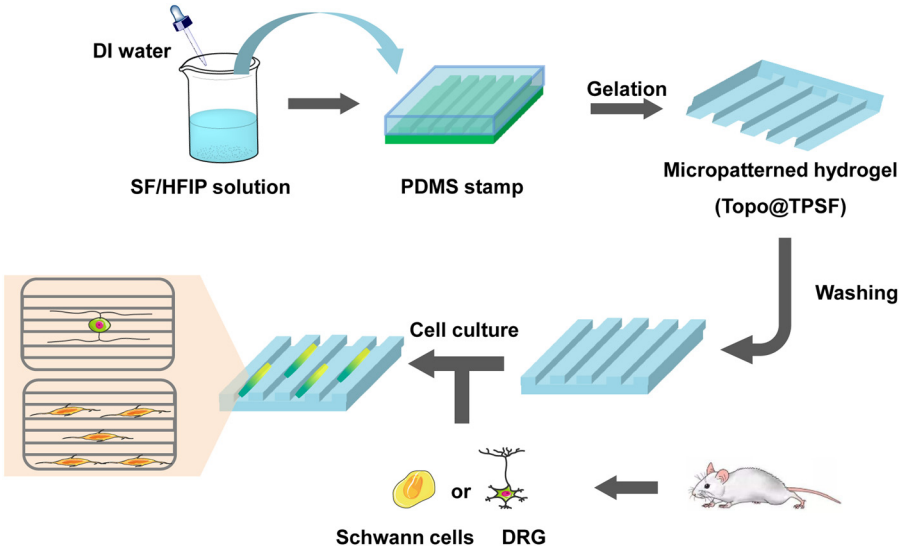

Scheme 1: Schematic illustration of Topo@TPSF hydrogel with aligned microgrooved structures for promoting cell growth and guiding neurite sprouting.

SF was dried in the air at room temperature. 20% w/v of SF was dissolved in 9.3 M LiBr solution and stirred at 60°C for 3 h and then dialyzed in ultrapure water for 3 days. Finally, the SF powder can be obtained by lyophilization, 0.45 g lyophilized SF powder was dissolved in 3 mL HFIP and then 2.7 mL ultrapure water was slowly added into the solution. The SF/HFIP/water solution was then transferred into a mold and incubated for 24 h in a sealed environment. After gelation, the hydrogels were washed in ultra-pure water at 80°C to remove HFIP.

For Topo@TPSF hydrogels, the SF/HFIP/water solution was then transferred into a mold with a PDMS stamp with surface ridge/groove microstructure and incubated for 24 h in a sealed environment. After gelation, the PDMS stamp was peeled-off and the hydrogels were washed in ultra-pure water at 80°C to remove HFIP.

2.2 Mechanical evaluation

The compressive-strength evaluation was investigated by an electronic universal testing machine (UTM; TFW-58; Shanghai Tuofeng Instrument Technology Co. Ltd, Shanghai, China). Hydrogel samples were cut into the shape of a solid cylinder with 20 mm diameter and 8 mm

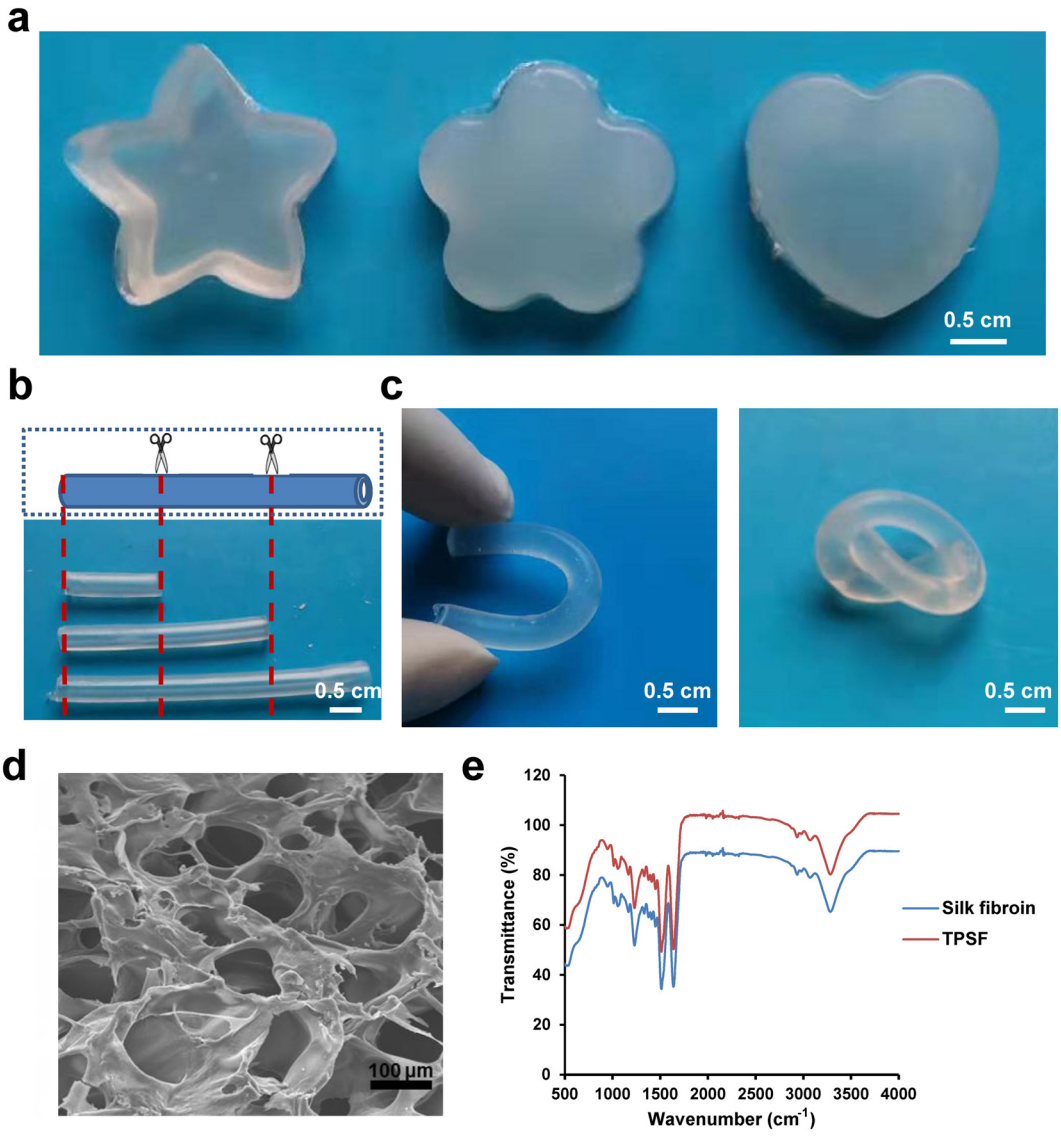

Figure 1: Characterization of TPSF hydrogel: (a) visual image of hydrogels with various 3D structures, (b) scale bar: 0.5 cm, (c) photographs of the cutting, bending, and knotting shapes of hydrogels, (d) SEM image of TPSF hydrogel, and (e) FTIR spectra of TPSF hydrogel.

thickness and tested at a displacement rate of 5 mm min^{-1}. The stress at 25% strain of each sample was recorded and Young's modulus was calculated from the slope of stress–strain curve.

2.3 Hydrophilic analysis

The hydrophilicity of hydrogels was evaluated using a contact angle instrument (JYPHa, Chengde, China). A droplet of water was dropped onto the hydrogel surface, and the angle formed between the water and the surface of the hydrogel was measured.

2.4 Evaluation of porosity

Freeze-dried hydrogels were immersed in anhydrous ethanol with a known volume (V_1). Then, the mixture was evacuated at 0.08 kPa and the volume of the ethanol

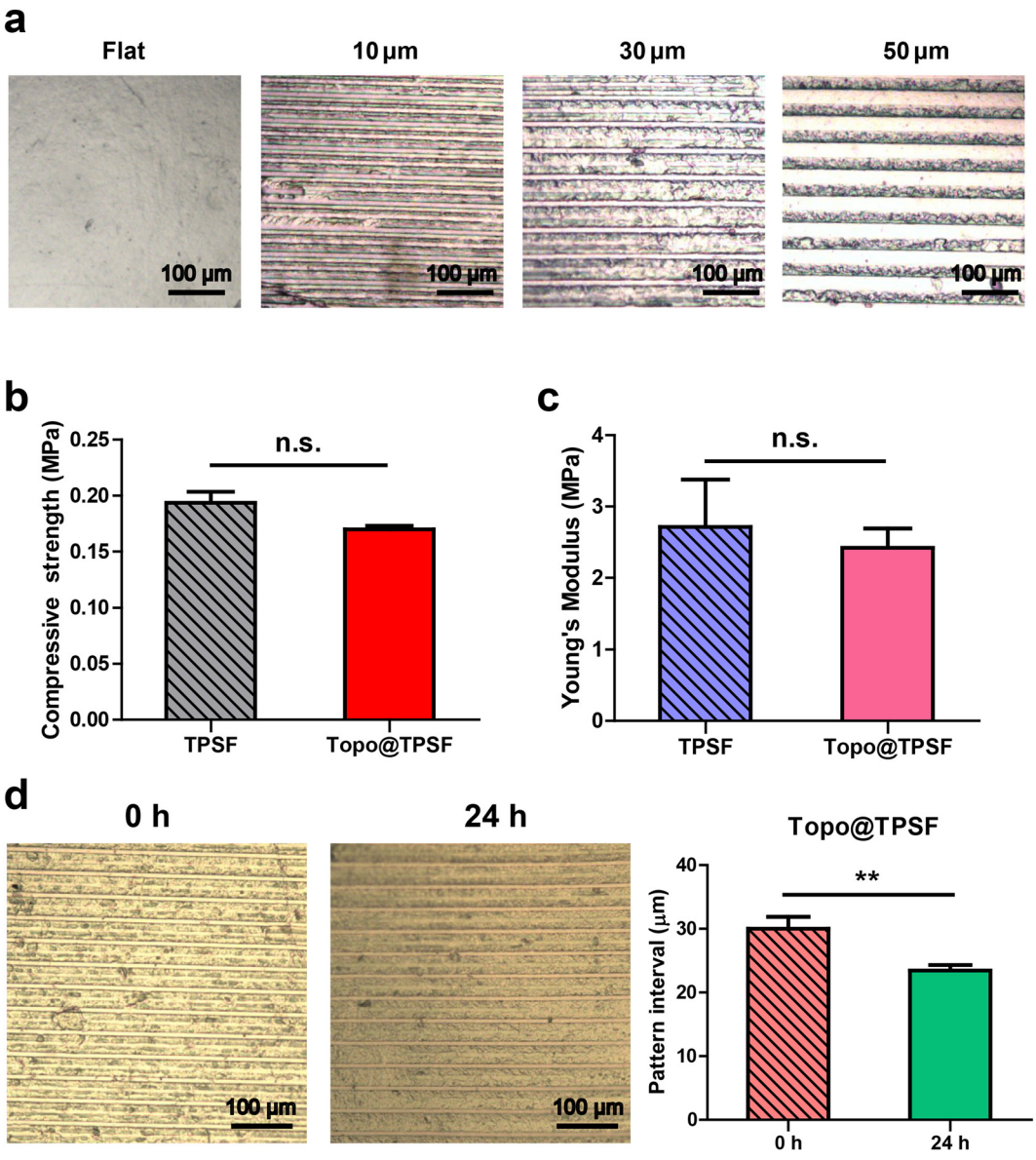

Figure 2: Surface topology and mechanical property of hydrogels. (a) Microscopic image of aligned micro-grooved structures on the surface of Topo@TPSF hydrogels. Scale Bar: 100 μm. (b) Compressive strengths of hydrogels. Data represent the mean ± S.E.M., ($n = 4$). (c) Young's modulus of hydrogels. Data represent the mean ± S.E.M., ($n = 4$). (d) Stability of microstructures. Data represent the mean ± S.E.M., ($n = 7$), $^{**}p < 0.01$.

was recorded as V_2, and after removal of the hydrogels, the volume of the remaining ethanol was recorded as V_3. Porosity was calculated, as follows:

$$P = (V_1 - V_3)/(V_2 - V_3) \times 100\%.$$

2.5 Schwann cells culture

The sterilized hydrogels were placed in a 24-well plate and then Schwann cells from Sprague–Dawley rat pups (1 day old) with a density of 1×10^5 cells/mL in DMEM were seeded onto the hydrogels and incubated at 37°C for 3 days. A live/dead cytotoxicity kit (Molecular Probes, USA) was utilized to visualize the cell behavior. The cytotoxicity of the hydrogels was assessed by the cell counting kit-8 (CCK-8) (Beyotime Biotechnology, China).

2.6 Dorsal root ganglion (DRG) culture

The sterilized hydrogels were placed in a 24-well plate, and DRG obtained from the spinal cord of 1-day-old rats was cultured on the SF hydrogels directly without digestion for 3 days. A live/dead cytotoxicity kit was utilized to visualize the cell behavior.

3 Results and discussion

3.1 Characterization of hydrogel

Tough pure-silk fibroin hydrogel (TPSF) was prepared by binary-solvent-induced conformation transition strategy [34]. Figure 1a shows that TPSF hydrogel can uniformly fit various shapes after curing. Fine mechanical properties are important for scaffolds to adapt to dynamic movement *in vivo* [36]. Then, the flexible mechanical properties of TPSF hydrogel in various shapes, even after cutting, bending, and knotting are demonstrated in Figure 1b andc. The SEM image in Figure 1d shows that the TPSF hydrogel exhibits a porous structure, which is critical for hydrogel use as biomaterials [37]. Then, the chemical structures of TPSF hydrogel were confirmed by Fourier

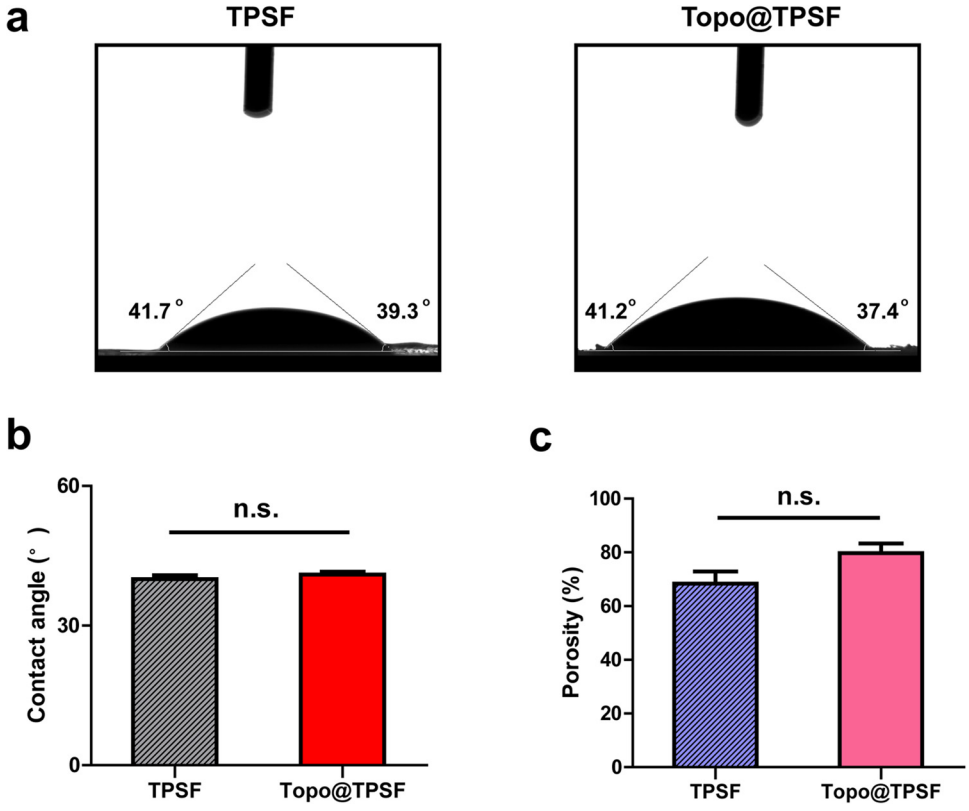

Figure 3: Contact angle and porosity of hydrogels: (a) and (b) contact angle of hydrogels and (c) porosity of hydrogels. Data represent the mean ± S.E.M., (n = 5).

transform infrared spectroscopy (FTIR) analysis, characteristic peak of SF was observed at 1,624 cm^{-1}, which represented the β-sheet in amide I region [38].

3.2 Mechanical property and surface topology

Grooved structures are considered very effective in promoting axonal guidance, as they can provide more sensing targets and appropriate contact areas for the growth cones of neuritis [46]. Micropatterned pure-SF hydrogels (Topo@TPSF) were successfully fabricated by *in situ* micromolding with PDMS stamps. Topo@TPSF hydrogels demonstrated regular aligned microgrooved structures with a width of 10, 30, and 50 μm, which all had clear edges as shown in Figure 2a and Figure S1. To further investigate the stability of aligned micro-grooved structure on Topo@TPSF hydrogel, the hydrogels were immersed in PBS at 37°C for 24 h. As shown in Figure 2d, micropatterns maintained in good shape with clear edges, indicating that the Topo@TPSF hydrogel had good stability. Appropriate mechanical properties of hydrogels are important for implants used for nerve regeneration [39]. Therefore, the compressive strength was evaluated. The representative stress–strain curves of compressive strength are plotted in Figure S8. As shown in Figure 2b and c, the compressive strength of hydrogels was in the range from 0.15 to 0.2 MPa and the Young's modulus of TPSF and Topo@TPSF was 2.7 ± 0.7 and 2.4 ± 0.3 MPa, respectively. These results illustrate that these hydrogels hold desirable mechanical properties for potential *in vivo* applications within the range of Young's modulus of human tissues (1–100 kPa) [40].

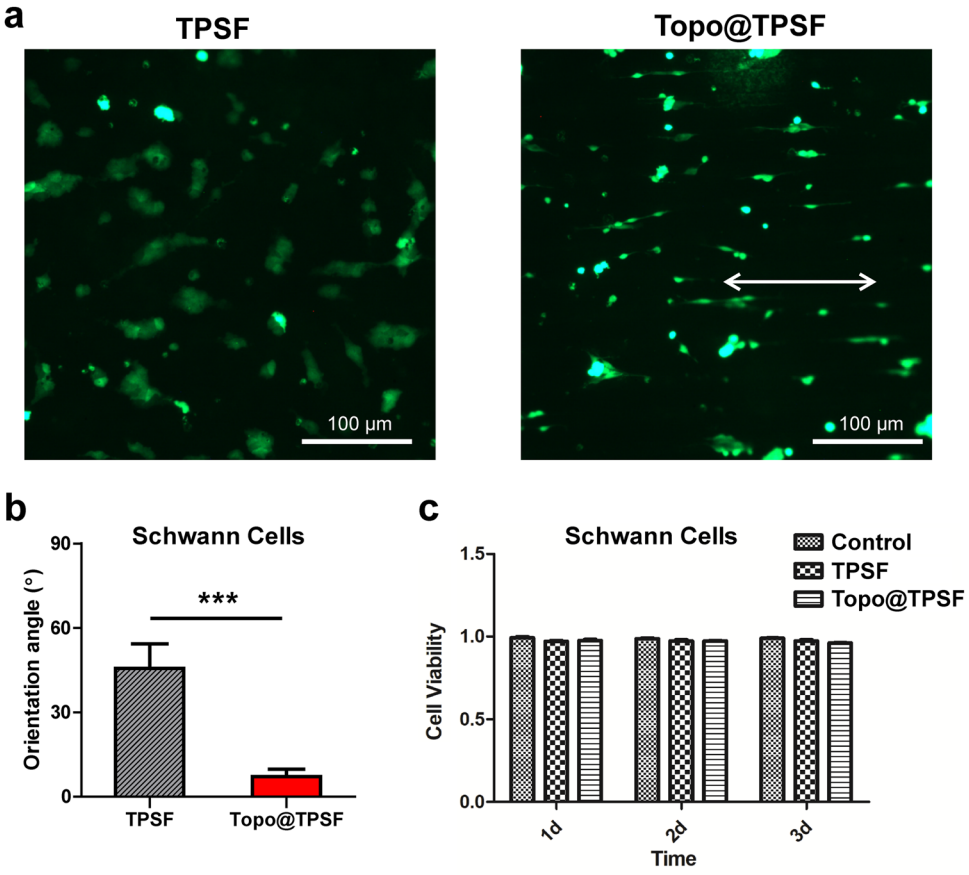

Figure 4: Schwann cell behavior on hydrogels and *in vitro* cytotoxicity. (a) Fluorescence images of Schwann cells cultured on hydrogels after 24 h of incubation. (b) Orientation angle of Schwann cells. Data represent the mean ± S.E.M., ($n = 5$). ***$p < 0.001$. (c) Viability of Schwann cells cultured on hydrogels for 3 days. Data represent the mean ± S.E.M., ($n = 3$).

3.3 Wettablity and porosity

Surface wettability reveals the hydrophilicity of biomaterials, which affects their biocompatibility [41]. Then, the wettability of the hydrogels was evaluated by measuring the contact angle (θ) of water droplets on the surface of hydrogels. It was found that the contact angles were all <90°, indicating that the hydrogels exhibited good hydrophilicity (see Figure 3a and b). The contact angles of water droplets on the surface of Topo@TPSF hydrogel with a groove width of 10, 30, and 50 μm were further measured. It was found that there is no significant difference between hydrogels with three different dimensions, due to the wettability of hydrogels which may mainly depend on the good hydrophilicity of SF (Figure S7). The porosity of a hydrogel also plays a major role in tissue regeneration [42]. As shown in Figure 3c, both TPSF and Topo@TPSF hydrogels held high porosity, which allows the exchange of nutrition and metabolism during tissue growth.

3.4 Schwann cell behavior and cytotoxicity

Silk-based materials have shown a promising capability to sustain Schwann cell growth for nerve repair [43]. Previously, it was also found that polyacrylamide hydrogel with a stable and clear surface groove structure of 30 μm pave the way for effectively guiding the cell growth of Schwann cells [22]. Therefore, the behavior of Schwann cells on both TPSF hydrogel and Topo@TPSF hydrogel with a groove width of 30 μm was investigated. As shown in Figure 4a and b, Schwann cells were well attached and

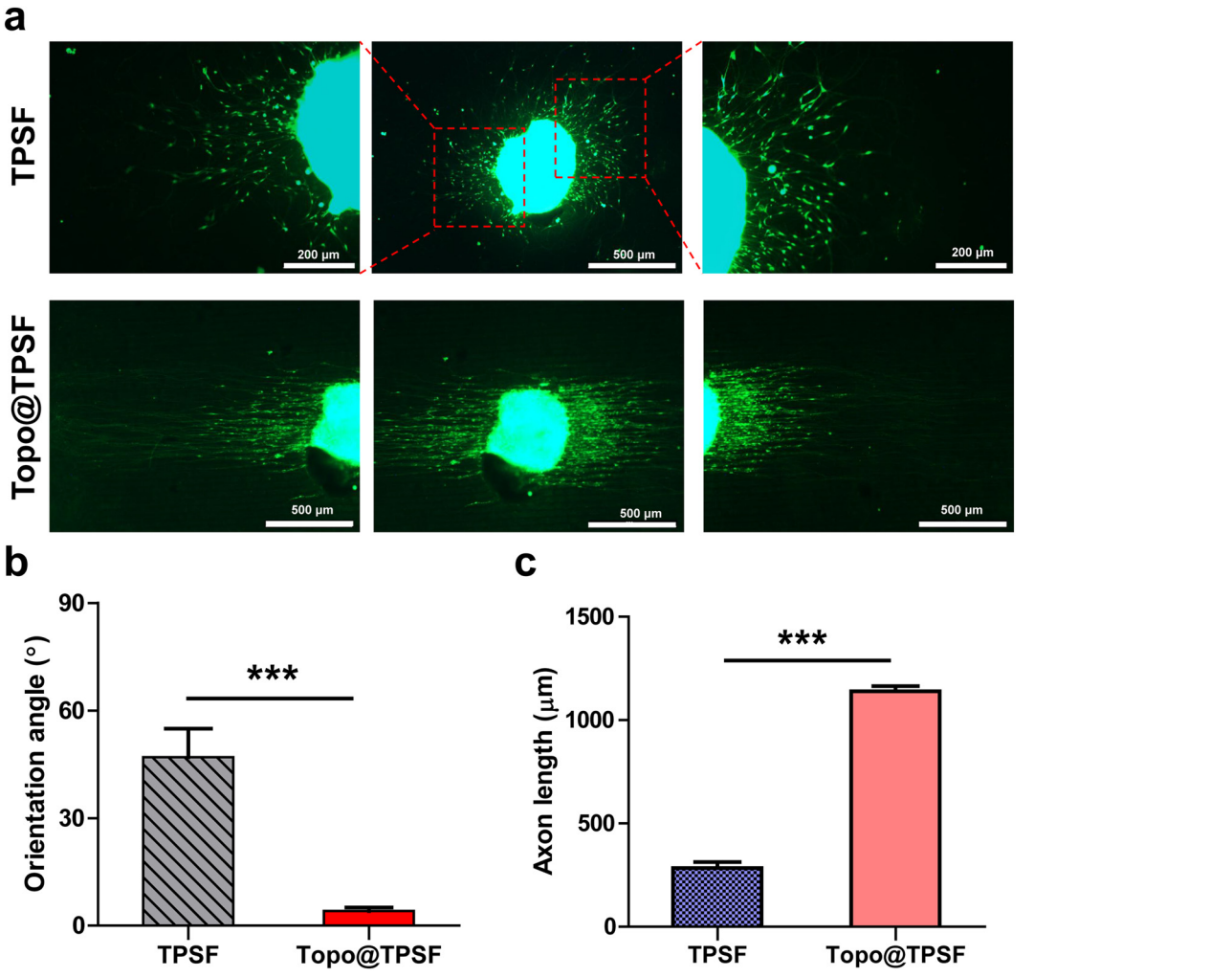

Figure 5: Neurite sprouting on hydrogels: (a) fluorescence images of DRG cultured on hydrogels after 3 days of incubation, (b) orientation angle of neurites, and (c) axon growth of DRG cultured on hydrogels. Data represent the mean ± S.E.M., (n = 5). ***p < 0.001.

exhibited spindle shape morphology on the surface of the hydrogels after 24 h of incubation. Importantly, Schwann cells on Topo@TPSF hydrogel showed alignment growth with a much smaller orientation angle (7.2 ± 2.6°), while those cells on TPSF without micropatterns spread in a random orientation. Additionally, the Schwann cells on Topo@TPSF showed a much larger L/W ratio than those on TPSF, as shown in Figure S2. These results indicate that Topo@TPSF hydrogel possesses a promising capacity to guide the growth of Schwann cells. The ability of biomaterials to allow cells to survive and grow is fundamental to tissue repair and regeneration [44]. To evaluate the biocompatibility of hydrogels with Schwann cell, cck8 assays were performed to evaluate the cell viability. The results showed that both the hydrogels were biocompatible (cell viability: >95%) (Figure 4c). To further confirm the biocompatibility of hydrogels, L929 cells were incubated with hydrogel for 3 days and stained with a live/dead cytotoxicity kit. As shown in Figure S3, very few dead cells were found on hydrogels, indicating the good biocompatibility of these hydrogels.

3.5 DRG behavior

Rapid regeneration of axons along the orientation of scaffolds is key for repairing long-distance nerve defects [45]. To assess the guidance potential of Topo@TPSF hydrogel with a groove width of 10, 30, and 50 μm, DRG neurons were cultured on hydrogels and the neurite extension *in vitro* on these hydrogels was evaluated. As shown in Figure 5a and Figure S4, neurons adhered to Topo@TPSF hydrogels with a groove width of 10, 30, and 50 μm all exhibit extensive and aligned neurite sprouting along the direction of microgrooves. Especially, the average axon length of neurons on Topo@TPSF hydrogels with a groove width of 30 μm was much longer than those on hydrogels of the other dimensions (Figure S5). Meanwhile, Topo@TPSF hydrogels with a groove width of 30 μm showed the most effective capacity on guiding neurite sprouting with lowest neurites orientation angle (<10°) (Figure S6). In contrast, neurons that adhere to the TPSF hydrogel without micropatterns extend neurite in all directions. In Figure 5b, the orientation angle of aligned neurite on Topo@TPSF was 4.1 ± 1.0°, whereas, neurons cultured on TPSF hydrogels show a much larger neurite orientation angle of 47.0 ± 8.0° with the extremely random state. The average length of axon on the Topo@TPSF hydrogels was much higher than those on the TPSF hydrogel without micropatterns (Figure 5c). As rapid axon growth is a key to accelerate nerve regeneration for the successful repair of long-distance peripheral nerve injuries (>40 mm), the average length of axon Topo@TPSF hydrogel with a groove width of 30 μm was about four-fold longer than that on TPSF hydrogel. These results demonstrate that Topo@TPSF hydrogels hold strong capacity of promoting axon growth and guiding neurite sprouting for potentially applying on repairing long-distance peripheral nerve injuries.

4 Conclusion

In summary, a high-strength micropatterned SF hydrogel without a chemical crosslink agent was developed. The hydrogels exhibit excellent mechanical properties of good flexibility and high strength. It terms of biocompatibility, the hydrogels possess good hydrophilicity and support cell attachment and cell survival. Significantly, the hydrogel with aligned microgrooved structures can successfully regulate the growth of Schwann cells, promote axon growth, and guide neurite sprouting. Therefore, the authors believe that this novel SF hydrogel would provide a promising tool for peripheral nerve regeneration.

Funding information: The authors gratefully acknowledge the financial support of the National Key Research and Development Program of China (2018YFC1105600).

Author contributions: Xinyi Gu and Xiaoli Chen contributed equally to this work. All authors have accepted responsibility for the entire content of this manuscript and approved its submission.

Conflict of interest: The authors state no conflict of interest.

References

[1] Sarker MD, Naghieh S, McInnes AD, Schreyer DJ, Chen X. Regeneration of peripheral nerves by nerve guidance conduits: Influence of design, biopolymers, cells, growth factors, and physical stimuli. Prog Neurobiol. 2018;171:125–50.
[2] Liu Y, Liu J, Chen S, Lei T, Kim Y, Niu S, et al. Soft and elastic hydrogel-based microelectronics for localized low-voltage neuromodulation. Nat Biomed Eng. 2019;3(1):58–68.
[3] Li R, Li D, Wu C, Ye L, Wu Y, Yuan Y, et al. Nerve growth factor activates autophagy in Schwann cells to enhance myelin

debris clearance and to expedite nerve regeneration. Theranostics. 2020;10(4):1649–77.
[4] Ray WZ, Mackinnon SE. Management of nerve gaps: Autografts, allografts, nerve transfers, and end-to-side neurorrhaphy. Exp Neurol. 2010;223(1):77–85.
[5] Yi S, Xu L, Gu X. Scaffolds for peripheral nerve repair and reconstruction. Exp Neurol. 2019;319:112761.
[6] Tajdaran K, Chan K, Gordon T, Borschel GH. Matrices scaffolds, and carriers for protein and molecule delivery in peripheral nerve regeneration. Exp Neurol. 2019;319:112817.
[7] Cai S, Wu C, Yang W, Liang W, Yu H, Liu L. Recent advance in surface modification for regulating cell adhesion and behaviors. Nanotechnol Rev. 2020;9(1):971–89.
[8] Kim JI, Hwang TI, Lee JC, Park CH, Kim CS. Regulating electrical cue and mechanotransduction in topological gradient structure modulated piezoelectric scaffolds to predict neural cell response. Adv Funct Mater. 2020;30(3):1907330.
[9] Bosi S, Fabbro A, Ballerini L, Prato M. Carbon nanotubes: a promise for nerve tissue engineering. Nanotechnol Rev. 2013;2(1):47–57.
[10] Martinez-Perez CA. Electrospinning: a promising technique for drug delivery systems. Rev Adv Mater Sci. 2020;59(1):441–54.
[11] Huang Z, Tsui GC-P, Deng Y, Tang C-Y. Two-photon polymerization nanolithography technology for fabrication of stimulus-responsive micro/nano-structures for biomedical applications. Nanotechnol Rev. 2020;9(1):1118–36.
[12] Hu Y, Wu Y, Gou Z, Tao J, Zhang J, Liu Q, et al. 3D-engineering of cellularized conduits for peripheral nerve regeneration. Sci Rep. 2016;6:32184.
[13] Li G, Li S, Zhang L, Chen S, Sun Z, Li S, et al. Construction of biofunctionalized anisotropic hydrogel micropatterns and their effect on Schwann cell behavior in peripheral nerve regeneration. ACS Appl Mater Interfaces. 2019;11(41):37397–410.
[14] Ahmad SI, Hamoudi H, Abdala A, Ghouri ZK, Youssef KM. Graphene-reinforced bulk metal matrix composites: synthesis, microstructure, and properties. Rev Adv Mater Sci. 2020;59(1):67–114.
[15] Li G, Zhao X, Zhang L, Yang J, Cui W, Yang Y, et al. Anisotropic ridge/groove microstructure for regulating morphology and biological function of Schwann cells. Appl Mater Today. 2020;18:100468.
[16] Qiu X, Xu S, Hao Y, Peterson B, Li B, Yang K, et al. Biological effects on tooth root surface topographies induced by various mechanical treatments. Colloids Surf B Biointerfaces. 2020;188:110748.
[17] Muthukumar T, Sreekumar G, Sastry TP, Chamundeeswari M. Collagen as a potential biomaterial in biomedical applications. Rev Adv Mater Sci. 2018;53(1):29–39.
[18] Huang W, Ling S, Li C, Omenetto FG, Kaplan DL. Silkworm silk-based materials and devices generated using bio-nanotechnology. Chem Soc Rev. 2018;47(17):6486–504.
[19] Li J, Tang X, Zhu P, Zhao Y, Ling J, Yang Y. Preparation of chitosan scaffolds with various molecular weights and their enzymatic degradation *in vitro*. J Biomater Tiss Eng. 2018;8(12):1725–34.
[20] Ahmed A, Wang X, Yang M. Biocompatible materials of pulsatile and rotary blood pumps: a brief review. Rev Adv Mater Sci. 2020;59(1):322–39.
[21] Ma H, Zhou Q, Chang J, Wu C. Grape seed-inspired smart hydrogel scaffolds for Melanoma therapy and wound healing. ACS Nano. 2019;13(4):4302–11.
[22] Cheng L, Cai Z, Ye T, Yu X, Chen Z, Yan Y, et al. Injectable polypeptide–protein hydrogels for promoting infected wound healing. Adv Funct Mater. 2020;30(25):2001196.
[23] Chouhan D, Mandal BB. Silk biomaterials in wound healing and skin regeneration therapeutics: from bench to bedside. Acta Biomater. 2020;103:24–51.
[24] Jian W, Hui D, Lau D. Nanoengineering in biomedicine: current development and future perspectives. Nanotechnol Rev. 2020;9(1):700–15.
[25] Altman GH, Diaz F, Jakuba C, Calabro T, Horan RL, Chen JS, et al. Silk-based biomaterials. Biomaterials. 2003;24(3):401–16.
[26] Yi B, Zhang H, Yu Z, Yuan H, Wanga X, Zhang Y. Fabrication of high performance silk fibroin fibers via stable jet electrospinning for potential use in anisotropic tissue regeneration. J Mater Chem B. 2018;6(23):3934–45.
[27] Luan C, Liu P, Chen R, Chen B. Hydrogel based 3D carriers in the application of stem cell therapy by direct injection. Nanotechnol Rev. 2017;6(5):435–48.
[28] Donate R, Monzon M, Aleman-Dominguez ME, Ortega Z. Enzymatic degradation study of PLA-based composite scaffolds. Rev Adv Mater Sci. 2020;59(1):170–5.
[29] Chen Z, Zhang Q, Li H, Wei Q, Zhao X, Chen F. Elastin-like polypeptide modified silk fibroin porous scaffold promotes osteochondral repair. Bioact Mater. 2021;6(3):589–601.
[30] Magaz A, Faroni A, Gough JE, Reid AJ, Li X, Blaker JJ. Bioactive silk-based nerve guidance conduits for augmenting peripheral nerve repair. Adv Healthc Mater. 2018;7(23):1800308.
[31] Xuan H, Tang X, Zhu Y, Ling J, Yang Y. Freestanding hyaluronic acid/silk-based self-healing coating toward tissue repair with antibacterial surface. ACS Appl Bio Mater. 2020;3(3):1628–35.
[32] Chen S, Liu S, Zhang L, Han Q, Liu H, Shen J, et al. Construction of injectable silk fibroin/polydopamine hydrogel for treatment of spinal cord injury. Chem Eng J. 2020;399:125795.
[33] Zhang L, Xu L, Li G, Yang Y. Fabrication of high-strength mecobalamin loaded aligned silk fibroin scaffolds for guiding neuronal orientation. Colloids Surf B Biointerfaces. 2019;173:689–97.
[34] Zhu Z, Ling S, Yeo J, Zhao S, Tozzi L, Buehler MJ, et al. High-strength, durable all-silk fibroin hydrogels with versatile processability toward multifunctional applications. Adv Funct Mater. 2018;28(10):1704757.
[35] Zhao Y, Nakajima T, Yang JJ, Kurokawa T, Liu J, Lu J, et al. Proteoglycans and glycosaminoglycans improve toughness of biocompatible double network hydrogels. Adv Mater. 2014;26(3):436–42.
[36] Li J, Celiz AD, Yang J, Yang Q, Wamala I, Whyte W, et al. Tough adhesives for diverse wet surfaces. Science. 2017;357(6349):378–81.
[37] Zhang L, Liu T, Xie Y, Zeng Z, Chen J. A new classification method of nanotechnology for design integration in biomaterials. Nanotechnol Rev. 2020;9(1):820–32.
[38] Xu L, Sun YX, Niu CM, Ge R, Zhang L, Yang Y-M. Optimization preparation of silk fibroin nerve scaffolds. J Biomater Tissue Eng. 2018;8(1):117–23.

[39] Kharazi AZ, Dini G, Naser R. Fabrication and evaluation of a nerve guidance conduit capable of Ca^{2+} ion release to accelerate axon extension in peripheral nerve regeneration. J Biomed Mater Res Part A. 2018;106(8):2181–9.
[40] Yu Y, Yuk H, Parada GA, Wu Y, Liu X, Nabzdyk CS, et al. Multifunctional "Hydrogel skins" on diverse polymers with arbitrary shapes. Adv Mater. 2019;31(7):1807101.
[41] Xing F, Zhou C, Hui D, Du C, Wu L, Wang L, et al. Hyaluronic acid as a bioactive component for bone tissue regeneration: fabrication, modification, properties, and biological functions. Nanotechnol Rev. 2020;9(1):1059–79.
[42] Tang X, Gu X, Wang Y, Chen X, Ling J, Yang Y. Stable antibacterial polysaccharide-based hydrogels as tissue adhesives for wound healing. RSC Adv. 2020;10(29):17280–7.
[43] Wang Y, Kong Y, Zhao Y, Feng Q, Wu Y, Tang X, et al. Electrospun, reinforcing network-containing, silk fibroin-based nerve guidance conduits for peripheral nerve repair. J Biomater Tissue Eng. 2016;6(1):53–60.
[44] Peng Z, Tang P, Zhao L, Wu L, Xu X, Lei H, et al. Advances in biomaterials for adipose tissue reconstruction in plastic surgery. Nanotechnol Rev. 2020;9(1):385–95.
[45] Kaplan B, Merdler U, Szklanny AA, Redenski I, Guo S, Bar-Mucha Z, et al. Rapid prototyping fabrication of soft and oriented polyester scaffolds for axonal guidance. Biomaterials. 2020;251:120062.
[46] Wu T, Xue J, Xia Y. Engraving the surface of electrospun microfibers with nanoscale grooves promotes the outgrowth of neurites and the migration of schwann cells. Angew Chem Int Ed. 2020;132:2–9.